








## Magnetic properties of CoFeB films grown on a single-layer graphene underlayer

Imane Berrai <sup>1</sup>, Kyusup Lee <sup>2,3</sup>, Mohamed Belmeguenai <sup>1</sup>, Mingfang Cui,<sup>2</sup> Wafa Alimi,<sup>1</sup> Yves Roussigné <sup>1</sup>,  
Samir Farhat <sup>1</sup>, Hyunsoo Yang <sup>2</sup> and Salim Mourad Chérif <sup>1,\*</sup>

<sup>1</sup>Université Sorbonne Paris Nord, LSPM, CNRS, UPR 3407, F-93430 Villetaneuse, France

<sup>2</sup>Department of Electrical and Computer Engineering, National University of Singapore, 117576, Singapore

<sup>3</sup>Department of Physics, Pukyong National University, Busan 48513, Republic of Korea



(Received 6 September 2023; revised 12 December 2023; accepted 4 January 2024; published 29 January 2024)

Associating thin ferromagnetic (FM) films with two-dimensional (2D) materials appears to be a promising approach for the next-generation spintronic devices. Consequently, the control of the magnetic phenomena in the FM/2D systems is of the utmost importance. We investigate in this paper the structural, static, and dynamic magnetic properties of SiO<sub>2</sub>/single-layer graphene (SLG)/CoFeB (3 nm ≤  $t_{\text{CFB}}$  ≤ 20 nm)/Cu (3 nm) structures and compared them with control samples, without the SLG underlayer. The single-layer characteristics of the synthesized graphene are deduced from Raman spectroscopy investigations. Vibrating sample magnetometry measurements allowed deducing the magnetization at saturation  $M_s$ , the coercive field  $H_c$ , and the magnetic dead layer thickness  $t_d$ . In the absence of SLG, the nominal thickness  $t_{\text{CFB}}$  is almost preserved, while  $t_d \approx 2$  nm was determined in presence of graphene. Here,  $H_c$  was found to increase in presence of SLG compared with the control structures, while  $M_s$  are comparable. Brillouin light scattering and microstrip FM resonance measurements were employed to investigate the dynamic magnetic properties of the samples. It was found that the magnetic anisotropy results from interface and volume contributions and that the largest interface anisotropy was observed in presence of SLG. Measurements of the spin waves nonreciprocity, related to the interfacial Dzyaloshinskii-Moriya interaction (iDMI), revealed weak iDMI in our samples. The magnetic damping in the SLG/CFB films was found to be dominated by the two-magnon contribution. No spin pumping was observed either without or with graphene. Our results highlight the influence of the graphene ripples on the magnetic properties of graphene/FM-based heterostructures.

DOI: [10.1103/PhysRevMaterials.8.014410](https://doi.org/10.1103/PhysRevMaterials.8.014410)

### I. INTRODUCTION

The control of the properties of magnetic materials is crucial for spintronic applications [1,2]. The usual approach combines ferromagnetic (FM) thin layers with different properties, highlighting the dominant role of interface phenomena [3], such as in FM/heavy metal (HM) heterostructures [4], taking advantage of the large spin-orbit coupling (SOC) of the HM materials. A possibility emerged more recently consisting of the association of FM layers with two-dimensional (2D) materials [5–7]. Indeed, 2D materials exhibit interesting characteristics for spintronics, especially strong spin signals and long spin diffusion length [8]. Interestingly, among the 2D materials, graphene (Gr) shows an impressive suitability for spintronics with demonstrated efficient spin transport and spin filtering, leading to high tunnel magnetoresistance ratios (TMR) [9], or for development of spintronics devices based on perpendicular spin sources as required, for instance, for perpendicular-magnetic random-access memory schemes [10]. In this context, the control of the interface effects is of utmost importance since they can strongly affect the surface magnetic properties of nanometer-thick FM film in FM/2D materials [5,6,11,12]. This occurs through interfacial interac-

tions, leading to the enhancement of the magnetic properties at the interfaces. Thus, the control of the FM/2D interface, including morphological, chemical, and electronic properties, is important to monitor interface magnetic phenomena, such as perpendicular magnetic anisotropy (PMA), damping and interface Dzyaloshinskii-Moriya interaction (iDMI), which are of great interest for next-generation spintronic devices. Indeed, these parameters are sensitive to the disorder, defects, and the arrangement of atoms at the interfaces. Their investigation in FM/2D structures through the study of their static and dynamic magnetic properties, in relation with their interface structure and morphology, is a timely topic.

In Gr/transition metal (TM) interfaces, it was reported that the presence of Gr can substantially alter the electronic and magnetic properties of TM atoms, which depends on the degree of hybridization between the metal  $3d$  and Gr  $\pi$  orbitals [13–15]. Strong PMA of Co/Gr structures was reported from both first-principles and experiments [11,16]. Magnetic damping was found, for instance, to increase in Gr flakes/Co structure [17] due to inhomogeneous broadening induced by sample imperfections, excluding the spin-pumping effect that one can observe in FM/HM systems [18]. Intrinsic SOC associated with induced surface defects from the growth of CoFeB (CFB) on Gr was invoked to explain the observed large modulation of the Gilbert damping [19]. Recently, Rashba-shift-induced spin pumping in single-layer

\*cherif@univ-paris13.fr

graphene (SLG)/CFB structures was reported and correlated with structural and nanoscale morphological properties monitored during sputter deposition of the CFB layer [20]. On another hand, calculations showed that the graphene coating of Co is found to induce a significant iDMI due to the Rashba effect [21], despite the weak SOC of Gr. Rashba-shift-induced iDMI was also reported [20]. Conversely, almost no iDMI for Co thin film deposited on Gr flakes was observed experimentally [17]. Recently, it has been shown that exfoliated *h*-BN transferred, under ultrahigh vacuum conditions, on ultrathin Co film induces large DMI and PMA [22], suggesting that the 2D/FM interface quality is of great importance. It is then essential to consider the morphological specificities of Gr, namely, the corrugations (wrinkles and ripples) that it forms, and to investigate their effect on the magnetic parameters mentioned above. Gr surface corrugations (wrinkles and ripples) have been reported in suspended Gr [23,24]. Indeed, 2D crystals are strictly unstable due to the thermodynamic requirement for the existence of out-of-plane bending with interatomic interaction generating a mathematical paradox [25]. The stability of the pseudo-2D material is achieved by ripple formation resulting from the partially decoupled bending and stretching modes [26,27]. Transmission electron microscopy experiments on suspended Gr showed the presence of ripples with height up to 1 nm [28]. Nanometer-sized ripples, like those found on freestanding Gr, were also reported in scanning-probe microscopy studies of Gr on SiO<sub>2</sub> substrates [29] or by scanning tunnelling spectroscopy measurements of Gr on Cu [30]. In this context, it is important to probe the effect of these corrugations on the magnetic parameters, particularly in the range of nanometric FM thicknesses. Our results, including the effect of ripples, are discussed subsequently in the light of studies addressing particularly the dynamic magnetic properties of Gr/FM-based systems.

We report in this paper on the effect of the Gr ripples on PMA, damping, and iDMI parameters in SLG/CoFeB (3 nm ≤  $t_{\text{CFB}}$  ≤ 20 nm)/Cu (3 nm) heterostructures. Chemical vapor deposition was used for the synthesis of Gr that we transferred to Si/SiO<sub>2</sub> substrates. CFB film of a given thickness was then grown on top of graphene and capped by a 3-nm-thick Cu layer, using physical vapor deposition (PVD). Reference samples without SLG were also elaborated for further comparison. The quality and domain size of graphene were deduced from Raman spectroscopy. The vibrating sample magnetometry (VSM) technique was used to study the static magnetic behaviors (saturation magnetization, coercive field, and magnetic dead layer) of the samples, while magnetic anisotropy and iDMI were deduced from the dynamic magnetic properties from spin-wave behavior using Brillouin light scattering (BLS) spectroscopy, and microstrip line FM resonance (MS-FMR) measurements were mainly used to analyze the magnetic damping.

## II. SAMPLES AND EXPERIMENTS

Series of samples Si/SiO<sub>2</sub>/SLG/Co<sub>20</sub>Fe<sub>60</sub>B<sub>20</sub>( $t_{\text{CFB}}$ )/Cu (3 nm) [Fig. 1(a)] and Si/SiO<sub>2</sub>/Co<sub>20</sub>Fe<sub>60</sub>B<sub>20</sub> (3 nm ≤  $t_{\text{CFB}}$  ≤ 20 nm)/Cu (3 nm) [Fig. 1(b)] were elaborated.

The Gr was synthesized using the inductive heating method using copper as a catalyst [31–33]. Heating of copper was

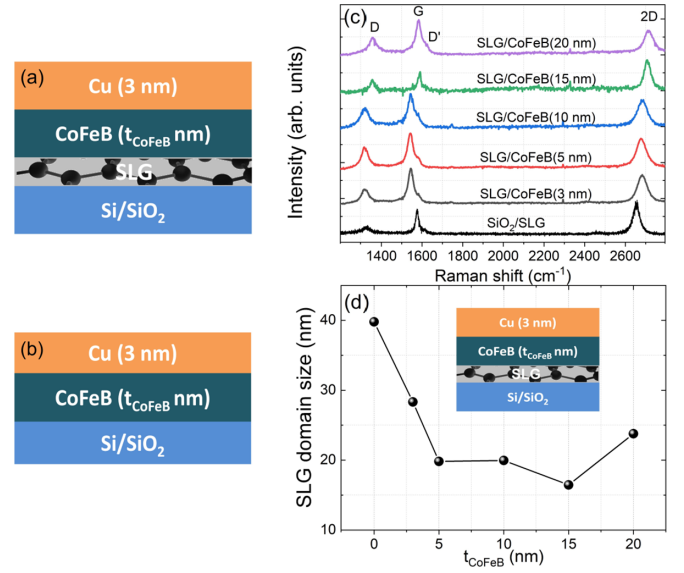


FIG. 1. Scheme of the (a) single-layer graphene (SLG)/CFB/Cu and (b) CFB/Cu samples. (c) Raman spectra of the SLG/CFB( $t$ )/Cu samples and (d) SLG domain sizes determined for the SLG/CFB samples; line is a guide for the eyes.

performed via magnetic induction, which involves a changing magnetic field in the radiofrequency mode. This allows for fast and localized heating, thereby reducing the heating time and improving thermal homogeneity. The different steps of this method are briefly exposed: (i) A methane flow is decomposed over the Cu substrate heated by magnetic induction to  $\sim 1035$  °C; (ii) the copper allows for significant reduction of the energy required to form strong Cu–CH<sub>*x*</sub> and Cu–H bonds; (iii) surface chemistry catalyzed by Cu allows graphene nucleation and growth; and (iv) carbon is deposited on the Cu substrate to form graphene over it. The step following graphene growth consists of removing the Cu substrate and transfer of graphene onto the whole surface of the Si/SiO<sub>2</sub> substrate. This is achieved, first, by spin-coating the sample with poly-methyl methacrylate (PMMA) and then removing of the Cu substrate by wet chemical etching, followed by transfer of the graphene/PMMA layer onto the Si/SiO<sub>2</sub> substrate. The PMMA is then removed using acetone. Note that we have previously reported the observation of Gr ripples formation, synthesized with our method, already at early stages of Gr synthesis [31].

Before CFB and Cu deposition under ultrahigh vacuum PVD, the samples were heated to 445 K for 5 min in the sputter chamber to desorb oxygen on Gr [34]. Deposition rates were  $\sim 1$  and 2.5 nm/min for CFB and Cu, respectively. The thickness control is ensured with quartz balance equipment with precision of  $\sim \pm 10\%$ . The crystalline quality and thickness of the as-grown Gr films were investigated by room-temperature (RT) Raman spectroscopy operating with a laser wavelength  $\lambda_{\text{RAMAN}} = 473$  nm. VSM measurements allowed determining the coercive field  $H_c$  and the saturation magnetic moment per unit area ( $M_s \times t_{\text{CFB}}$ ) that is used to obtain the  $M_s$  and the thickness of the magnetic dead layer ( $t_d$ ). BLS, operating with a laser wavelength  $\lambda_{\text{BLS}} = 532$  nm in the Damon-Eshbach configuration [35], was employed to

investigate the PMA, the magnetic damping, and the iDMI. Indeed, BLS provided information on the iDMI, through the investigation of the nonreciprocity of the spin waves (SWs) within the samples [36,37]. The BLS setup operates in the 3–100 GHz SW frequency range. The SW frequency can be studied as function of SW wave vector  $k$  in the range  $4\text{--}20\ \mu\text{m}^{-1}$ , related to the incident angle  $\theta$  through the relation  $k = 4\pi \sin(\theta)/\lambda_{\text{BLS}}$ , and of an in-plane applied magnetic field  $H$  up to 1.3 T. MS-FMR [38] was also used to investigate damping through the study of the frequency dependence of the FMR field linewidth ( $\Delta H$ ).

### III. RESULTS AND DISCUSSION

#### A. Raman measurements

Figure 1(c) shows the Raman spectra obtained from the as-grown graphene and the graphene/CFB samples. We observe the characteristic bands of graphene, namely, the G band ( $\sim 1583\ \text{cm}^{-1}$ ) and the 2D band ( $\sim 2667\ \text{cm}^{-1}$ ), together with the D band ( $\sim 1337\ \text{cm}^{-1}$ ) related to defects and disorder [39,40]. The G band originates from the stretching vibration in the  $sp^2$  carbon plane [40,41]. The 2D band is linked to the band structure of the graphene layers and originates from a double two-phonon resonance process [42]. One can also notice the presence of a D' band of a weak intensity, associated with an  $E$  symmetry mode, which is double degenerate; as such, a splitting is expected under uniaxial strain [43]. The intensity ratio  $I_D/I_G$  of band D to band G allows analyzing the quantity of defects in graphene [39], indicating in our case a good Gr structural quality with the presence of low-defect concentration since this ratio  $\sim 0.3$  fulfills the condition of being less than unity. Note that sputtering deposition of CFB may increase defects regarding the as-grown graphene. This latter is single layer (SL) since the  $I_{2D}/I_G$  intensity ratio is higher than unity, being  $\sim 1.3$  [44]. The observed shifts in phonon frequencies can be attributed to stress accompanying metal deposition onto the SLG [45]. The SLG domain size ( $L_a$ ) is estimated for as-grown Gr from the  $I_D/I_G$  ratio using [46]

$$L_a(\text{nm}) = (2.4 \times 10^{-10}) \lambda_{\text{RAMAN}}^4 (I_D/I_G)^{-1}. \quad (1)$$

This expression provides an estimation of  $L_a$  for the as-grown Gr alone and probably a rough estimation in the case of the SLG/CFB samples [Fig. 1(d)]. The domain size is found to be tens of nanometers, which may potentially impact interface magnetic effects in Si/SiO<sub>2</sub>/SLG/CFB/Cu heterostructures, as we discuss below.

#### B. Static magnetic properties

Figures 2(a) and 2(b) show two representative hysteresis loops recorded for the CFB films with nominal thicknesses  $t_{\text{CFB}} = 5$  and 15 nm, respectively, without and with SLG.

Note the enhancement of  $H_c$  in the presence of SLG, as depicted in Fig. 3(c). It is also worth noticing the peculiar behavior of the nominal  $t_{\text{CFB}} = 3$  nm film that showed a significant reduction in remanence and magnetization in the presence of SLG (see insert in Fig. 2). Pinning at Gr domain boundaries can be considered a driving mechanism

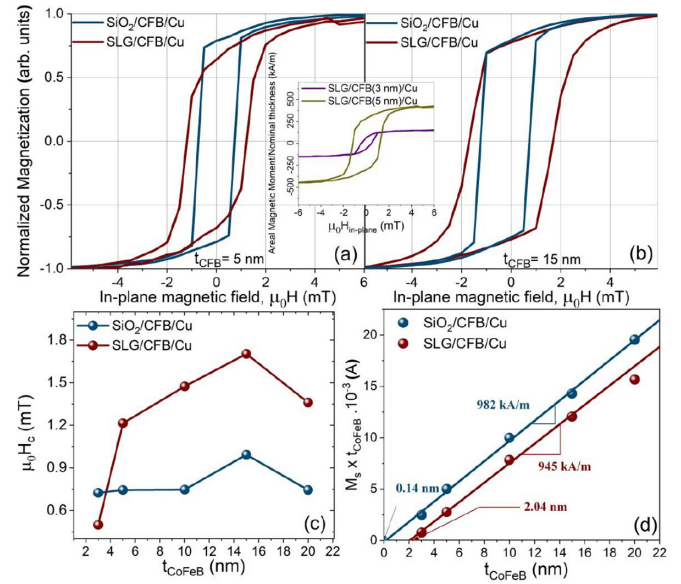


FIG. 2. (a) Vibrating sample magnetometry (VSM) loops of (a) CFB (5 nm) sample with or without single-layer graphene (SLG) underlayer, (b) CFB (15 nm) sample with or without SLG underlayer, (c) thickness dependence of coercive field  $\mu_0 H_c$ , (d) CFB thickness dependence of  $M_s \times t_{\text{CFB}}$ . Insert presents loops for SLG/CFB( $t_{\text{CFB}}$ )/Cu for nominal  $t_{\text{CFB}} = 3$  and 5 nm, respectively.

for coercivity [47]. In the case of the Gr/Co system, large three-dimensional (3D) clusters, with low density promoting multigrain films, were observed to initiate the growth of Co on Gr. Consequently, an increase in domain wall pinning likely contributes to  $H_c$  enhancement in the presence of Gr [48]. SOC may also play a role [49]. Roughness is also an important parameter determining the coercivity [50].

Usually, to quantify the magnetic interface effects, one varies the FM layer thickness. However, the presence of a magnetically dead layer ( $t_d$ ) can reduce the effective FM thickness  $t_{\text{eff}} = t_{\text{CFB}} - t_d$  [4]. The dead layer can be the consequence of interdiffusion between atoms of materials in contact with the FM layer and FM atoms. Another origin, when the material in contact with the FM layer is graphene, can be structural due to the presence of Gr ripples. The thickness of the magnetic dead layer ( $t_d$ ) and the magnetization at saturation ( $M_s$ ) should therefore be first determined to avoid incorrect estimates of the magnetic interface effects.

Figure 2(d) shows the typical dependence of the areal saturation magnetic moment ( $M_s \times t_{\text{CFB}}$ ) vs the CFB thickness for samples without and with the SLG underlayer. Here,  $M_s$  and  $t_d$  are determined from the linear fits: The slope indicates  $M_s$ , while the horizontal axis intercept indicates the extent of  $t_d$ . In the presence of SLG,  $t_d$  is estimated to be  $\sim 2$  nm, while it is 0.14 nm without the SLG underlayer. Such a value with SLG is consistent with the magnitude of the Gr ripples reported by Ishigami *et al.* [29] and Bai *et al.* [30]. Here,  $M_s$  is deduced to be  $\sim 982 \pm 50$  kA/m ( $945 \pm 50$  kA/m) in the absence (presence) of SLG, respectively. These values are comparable with  $M_s = 800\text{--}1100$  emu/cm<sup>3</sup> obtained by Jang *et al.* [51], Wang *et al.* [52], and Belmeguenai *et al.* [18]

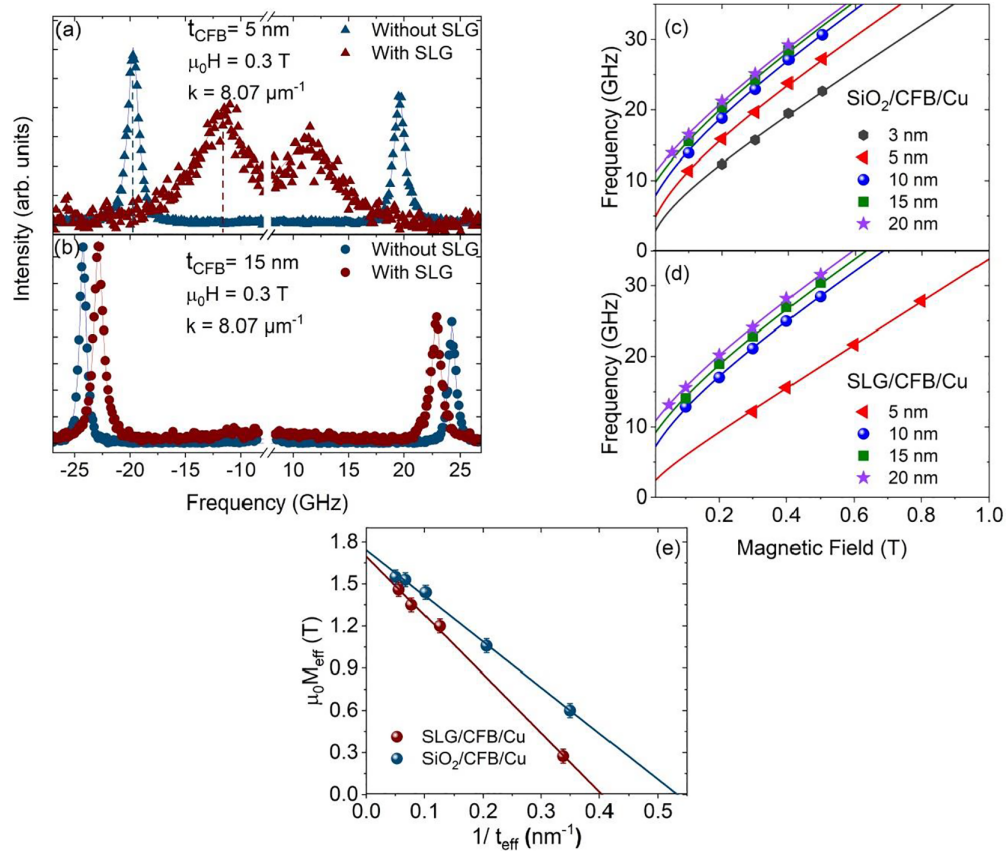


FIG. 3. BLS spectra: (a) CFB (5 nm) sample with or without single-layer graphene (SLG) underlayer, (b) CFB (15 nm) sample with or without SLG underlayer, (c) field dependence of the mean value of Stokes (S) and anti-Stokes (aS) frequencies in absence of SLG, (d) field dependence of the mean value of S and aS frequencies in presence of SLG, fitting curves obtained with Eq. (2) (see text), and (e) effective magnetization ( $\mu_0 M_{\text{eff}}$ ) vs the reciprocal effective thickness  $t_{\text{eff}}$  of CoFeB films with or without SLG underlayer.

but lower than that ( $M_s \approx 1200 \text{ emu/cm}^3$ ) of W/CoFeB/MgO [53] and Ta/CoFeB/Ta [54]. The dispersion in the value of  $M_s$  points out the fact that the magnetization of thin film strongly depends on its interfaces and the crystallization degrees of CoFeB. In our case, the amorphous state of the CoFeB layers is expected, as anticipated for our boron content (20%) [55]. Indeed, from x-ray diffraction measurements, the critical boron concentration at which CoFeB still crystallizes is estimated to be  $\sim 5\text{--}6\%$ .

### C. Dynamic magnetic properties

#### 1. Effective magnetization and magnetic anisotropies

To estimate the PMA, we have first conducted BLS experiments in the Damon-Eshbach configuration [35] which allows SW propagating along the in-plane direction perpendicular to the in-plane applied field  $H$  to be probed. The SW frequency shifts were determined from the Lorentzian fits of the BLS spectra. We have investigated the effective magnetizations

$\mu_0 M_{\text{eff}} = \mu_0 (M_s - H_{\perp})$ . Here,  $H_{\perp}$  is the PMA field extracted from the frequency variation vs the in-plane applied field. Also,  $H_{\perp}$  can be expressed as  $H_{\perp} = 2K_{\perp}/\mu_0 M_s$ , where  $K_{\perp}$  is the perpendicular anisotropy constant. BLS measurements were carried out at low wave vector ( $k = 8.07 \mu\text{m}^{-1}$ , i.e.,  $\theta = 20^\circ$ ) to avoid any possible contribution induced by the iDMI [56]. Figure 3(a) and 3(b) exhibits BLS spectra obtained for the nominal 5- and 15-nm-thick CFB films, respectively, in the presence or not of an SLG underlayer, with  $H = 0.3 \text{ T}$ . We can observe that, for the 5 nm sample, the width of the BLS lines is significantly enhanced in the presence of graphene. We have also obtained a very degraded signal for the nominal 3 nm sample with the SLG underlayer, probably due to the dead layer which significantly reduces the effective thickness of the CFB layer. Obviously, this effect is expected to be particularly pronounced for the thinnest films.

We obtained  $M_{\text{eff}}$  from the fit of the field dependence of the mean value of Stokes  $F_S$  and anti-Stokes  $F_{\text{aS}}$  frequencies, as depicted in Figs. 3(c) and 3(d), using

$$F = \left( \frac{F_S + F_{\text{aS}}}{2} \right) = \left( \frac{\mu_0 \gamma}{2\pi} \right) \sqrt{[H + Jk^2 + P(kt_{\text{eff}})M_s][H + Jk^2 - P(kt_{\text{eff}})M_s + M_{\text{eff}}]}, \quad (2)$$

where  $(\frac{\gamma}{2\pi})$  is equal to 30.13 GHz/T (i.e.,  $g = 2.15$ ) [57],  $H$  is the in-plane applied field,  $J = \frac{2A_{ex}}{M_s}$ , with  $A_{ex} = 10^{-11}$  J/m [58] the exchange stiffness constant of CFB, and  $P(kt_{eff})$  is a coefficient describing the dipolar interactions that reduces to  $P(kt_{eff}) \approx kt_{eff}/2$  in thin films verifying  $kt_{eff} \ll 1$  [57].

The obtained values of  $\mu_0 M_{eff}$  are shown in Fig. 3(e) vs the reciprocal CFB effective thickness  $1/t_{eff}$ . A linear dependence is observed. Here,  $K_{\perp}$  can be described by the phenomenological relationship  $K_{\perp} = K_v + \frac{K_s}{t_{eff}}$ ; thus, the linear fit of the thickness dependence of  $\mu_0 M_{eff}$  can provide the perpendicular uniaxial surface  $K_s$  and volume anisotropy  $K_v$  constants from the slope and the intercept with the vertical axis, respectively. We obtain  $K_s = (1.97 \pm 0.15)$  mJ/m<sup>2</sup> and  $K_v = (-2.39 \pm 0.21) \times 10^5$  J/m<sup>3</sup> for Si/SiO<sub>2</sub>/Gr/CFB/Cu, and  $K_s = (1.60 \pm 0.12)$  mJ/m<sup>2</sup> and  $K_v = (-2.49 \pm 0.21) \times 10^5$  J/m<sup>3</sup> for Si/SiO<sub>2</sub>/CFB/Cu. The volume anisotropy  $K_v$  constant is similar and negative for the two systems, reinforcing the magnetization lying spontaneously in the films plane. Here,  $K_v$  seems to not be influenced by the presence of the SLG. More significant difference is observed for the perpendicular uniaxial surface  $K_s$  constant that is reinforced in the presence of a SLG underlayer. The obtained  $K_s$  values are higher than those reported, for instance, for CoFeB/Pt ( $K_s = 1.3$  mJ/m<sup>2</sup>) [18] or CoFeB/Cu/Pt ( $K_s = 1.15 \pm 0.09$  mJ/m<sup>2</sup>) [59]. A certain degree of electron hybridization of  $3d$  Co and Fe orbitals with graphene  $\pi$  orbitals can be at the origin of the observed enhancement of the interface PMA in the presence of SLG [11,16,60]. In addition, if one considers the ripples as an interface roughness, the effect will be to reduce the shape anisotropy [61]. The anisotropy contribution resulting from the roughness will, therefore, always be positive, thus favoring PMA. It should be noted that the results of the effective magnetizations obtained by FMR are in good agreement with those determined by BLS [62]. They are not presented to avoid redundancy.

## 2. iDMI

iDMI is associated with the nonreciprocity of SWs having the same wavelength and propagating along two opposite directions through a magnetic material [36,37,63], resulting in a Stokes ( $F_S$ )/anti-Stokes ( $F_{AS}$ ) frequency difference ( $\Delta F = F_S - F_{AS}$ ). The iDMI value can thus be obtained using the relation  $F = \frac{2\gamma}{\pi M_s} D_{eff} k$ , where the effective iDMI constant  $D_{eff}$  characterizes the strength of iDMI. As an interface effect, iDMI scales linearly with the inverse thickness of the FM film.

Figure 4 exhibits BLS spectra obtained for the thinnest films, i.e., the nominal 5-nm-thick samples, at  $k = 20.45 \mu\text{m}^{-1}$ , corresponding to an incidence angle of the laser beam of 60°, the maximum value available from our BLS setup, where the iDMI effect, if present, is the highest. In the absence of the SLG underlayer, no measurable frequency mismatch is observed, likely due to the weak SOC at the CoFeB/Cu interface since Cu is a light element. A small  $\Delta F \sim 0.1$  GHz is observed in the presence of the SLG underlayer when reversing the sign of the applied field deducing  $D_{eff} = 0.038$  mJ/m<sup>2</sup>. Direct observation of unusual iDMI by BLS has been shown in graphene/NiFe/Ta heterostructures that increases with increasing the defect density of graphene obtained by varying argon pressure during sputter deposition

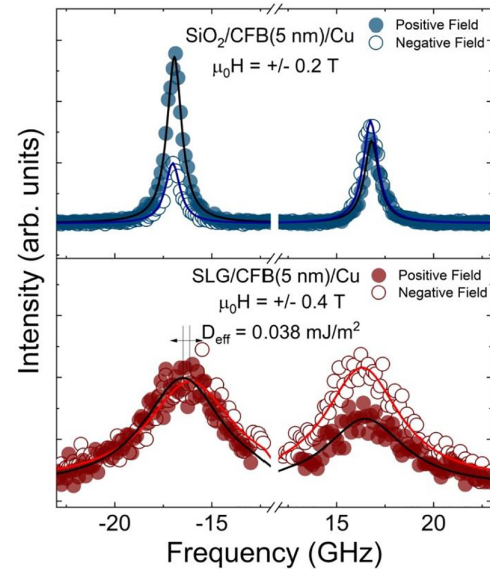


FIG. 4. Brillouin light scattering (BLS) spectra for CFB (5 nm) sample with and without single-layer graphene (SLG) underlayer taken at  $k = 20.45 \mu\text{m}^{-1}$ , corresponding to an incidence angle of the laser beam of 60°. Symbols refer to experimental data and solid lines are Lorentzian fits for positive and negative field allowing comparison of Stokes and anti-Stokes frequencies.

of Ni<sub>80</sub>Fe<sub>20</sub> [64], suggesting that the observed iDMI originates from defect-induced extrinsic SOC at the interface. A small iDMI of 0.07 mJ/m<sup>2</sup> was found for a 3 nm Fe<sub>20</sub>Ni<sub>80</sub> film. In SLG/CoFeB heterostructures, iDMI was correlated with structural and nanoscale morphological properties monitored during sputter deposition of the CoFeB layer, suggesting a dominant role of the Rashba shift and defect density in the emergence of iDMI [20]. No reference to a possible presence of a dead layer associated with Gr ripples had been mentioned in these studies. Note that, even if sputter deposition of CFB may increase defects regarding the as-grown graphene, as the Raman results suggest, this seems not to be sufficient to induce significant iDMI in our samples. In layered systems with broken structural inversion symmetry, it has been demonstrated that the iDMI is maximized when the quality parameter, defined as the difference between the roughness parameters, such as amplitude and period of the top and bottom interfaces of an FM layer, goes to zero [65,66]. This is probably not the case for our samples because the roughness at the bottom Gr/CFB interface, due to ripples, must be much higher than that at the top CFB/Cu interface, leading to weak iDMI. In ultrathin films composed of  $5d$  HM/FM/ $4d$ ( $5d$ ) HM or oxide interfaces, a clear effect of atomic-scale surface modulation on the magnetic properties and iDMI has been explained within a model of correlated roughness of interfaces [67]. When the amplitude and period of roughness are the same for both the top and bottom interfaces of the studied CoFeSiB-based systems, the CoFeSiB thickness remains unchanged, resulting in a value near the maximum iDMI value, which must be similar for ideally smooth interfaces. When the roughness amplitude for the top and bottom interfaces is different, there are local variations in the CoFeSiB layer thickness and, consequently, local variations in the iDMI.

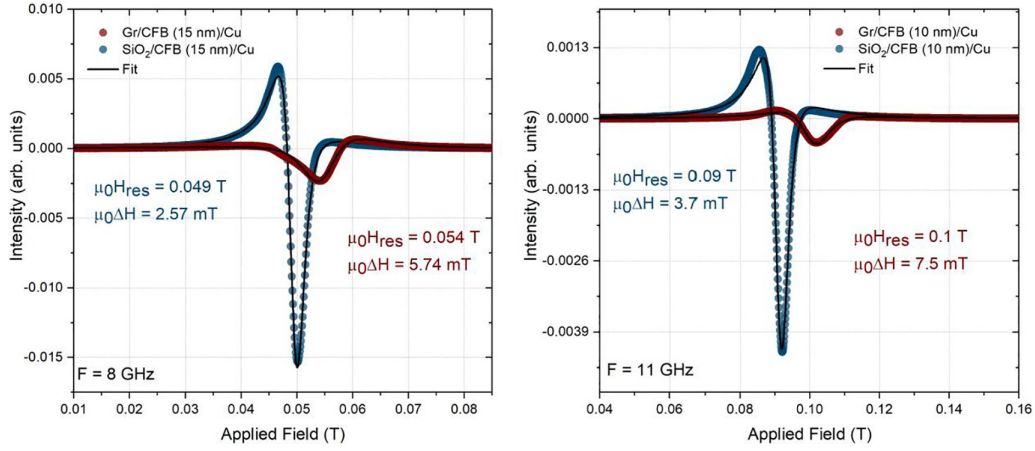


FIG. 5. Ferromagnetic resonance (FMR) spectrum obtained for the 10- and 15-nm-thick samples with and without single-layer graphene (SLG) underlayer; the fitting curves are obtained from Eq. (3).

#### IV. MAGNETIC DAMPING

We have investigated the magnetic damping using MS-FMR. Figure 5 illustrates representative FMR spectra with and without the presence of a SLG underlayer for the nominal  $t_{\text{CFB}} = 10$  and 15 nm samples. The resonance field ( $\mu_0 H_{\text{res}}$ ) and the half-line width ( $\mu_0 \Delta H$ ) were determined from fitting each spectrum using

$$\begin{aligned} \text{FMR}_{\text{signal}} = & a(\Delta H)(H - H_{\text{res}})[(H - H_{\text{res}})^2 + (\Delta H)^2]^{-2} \\ & + b[(H - H_{\text{res}})^2 - (\Delta H)^2] \\ & \times [(H - H_{\text{res}})^2 + (\Delta H)^2]^{-2} + c. \end{aligned} \quad (3)$$

The resonance field dependence of the frequency allowing determining the effective magnetization is presented in Ref. [62]. Good agreement is found with BLS ones.

We were interested in the effect of the presence of the SLG on the FMR field half-line width ( $\mu_0 \Delta H$ ) that results from extrinsic and intrinsic contributions to damping by analyzing the frequency dependence of  $\mu_0 \Delta H$  using

$$\mu_0 \Delta H = \mu_0 \Delta H_0 + \frac{\alpha f}{\gamma/2\pi}, \quad (4)$$

where  $\alpha$  is the Gilbert parameter,  $f$  is the driving frequency, and  $\mu_0 \Delta H_0$  is the inhomogeneous residual half-width, which is frequency independent. Figure 6 exhibits the experimental data (symbols) and the fittings (continuous lines) obtained from Eq. (4) (a) with and (b) without the SLG underlayer. The deduced values of  $\mu_0 \Delta H_0$  and  $\alpha$  are shown and commented on in Ref. [62].

The insertion of a Gr layer is found to significantly increase  $\mu_0 \Delta H_0$ , indicating the increase of heterogeneities. We conclude that the SLG layer is responsible for additional defects. Following Zhu *et al.* [68], the thickness dependence of the damping parameter [Fig. 6(c)] is analyzed using

$$\alpha = \alpha_0 + \alpha_1 t^{-1} + \alpha_2 t^{-2}. \quad (5)$$

Here,  $\alpha_0$  represents the intrinsic Gilbert damping,  $\alpha_1 t^{-1}$  corresponds to the spin pumping contribution, and  $\alpha_2 t^{-2}$  is related to the two-magnon scattering at interfaces.

The best fitting parameters for SLG/CFB samples are found to be  $\alpha_0 = 0.004$ ,  $\alpha_1 = 0$ , and  $\alpha_2 = 550 \text{ nm}^2$ , while for  $\text{SiO}_2/\text{CFB}$  ones,  $\alpha_0 = 0.004$ ,  $\alpha_1 = 0$ , and  $\alpha_2 = 180 \text{ nm}^2$ . The intrinsic damping constant  $\alpha_0$  is in line with values reported in literature:  $\alpha_{\text{CFB}} = 0.004$  for bulk  $\text{Co}_{20}\text{Fe}_{60}\text{B}_{20}$  [69],  $\alpha_{\text{CFB}} \approx (0.0034 \pm 0.0005)$  for CFB/Pt [18], and  $\alpha_{\text{CFB}} \approx (0.0031 \pm 0.0002)$  reported for CFB/ $\text{TaO}_x$  [70]. Interestingly, no spin pumping was observed either without or with graphene. This is not in line with the results reporting spin pumping in the SLG/CFB system that was correlated with the defect density present at the surface of the SLG [20]. Remarkably, in this latter study, the defect density had not been varied at constant

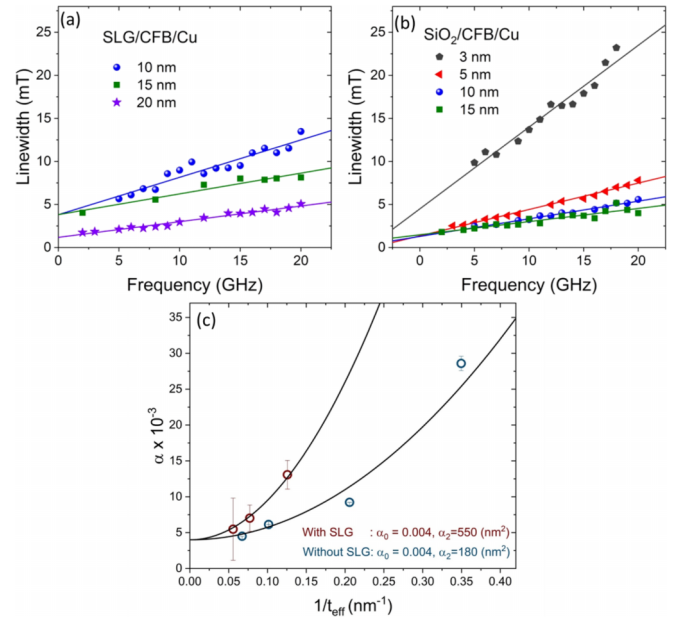


FIG. 6. Frequency dependence of  $\mu_0 \Delta H$  for (a) samples with single-layer graphene (SLG) and (b) control samples without SLG. Symbols refer to experimental data and continuous lines are fits obtained using Eq. (4) (see text). (c) Damping for  $\text{SiO}_2/\text{CFB}$  and SLG/CFB plotted as a function of  $t_{\text{eff}}^{-1}$ ; the fitting curves are obtained using Eq. (5) (see text).

thickness to establish a direct and unambiguous correlation. Notably, we observe in this paper that the insertion of a Gr layer significantly increases  $\alpha_2$ , i.e., the two-magnon contribution, in line with the results reported by Berger *et al.* [48] for the Gr/Co system. Based on our results, it is concluded that the SLG layer is responsible for introducing additional roughness, which is likely associated with the presence of graphene ripples.

## V. CONCLUSIONS

We prepared two series of heterostructures: Si/SiO<sub>2</sub>/graphene/Co<sub>20</sub>Fe<sub>60</sub>B<sub>20</sub>/Cu and Si/SiO<sub>2</sub>/Co<sub>20</sub>Fe<sub>60</sub>B<sub>20</sub>/Cu, with varying Co<sub>20</sub>Fe<sub>60</sub>B<sub>20</sub> thicknesses ranging from 3 to 20 nm. The quality of graphene layers was assessed using Raman spectra, confirming the SL character of graphene. Magnetometry, MS-FMR, and BLS techniques were used to investigate the magnetic properties of these samples. The magnetometry data revealed that graphene introduces a magnetic dead layer of  $\sim 2$  nm and increases the coercive field by  $\sim 0.7$  mT. Both MS-FMR and BLS measurements demonstrated an increase in surface magnetic anisotropy by  $\sim 0.4$  mJ/m<sup>2</sup>. MS-FMR measurements showed a significant increase in the two-magnon scattering contribution to the linewidth in the presence of the graphene layer but did not indicate any spin-pumping contribution. The two-magnon scattering contribution is amplified by a factor of three with the introduction of graphene. Additionally, counterpropagating

SWs, probed by BLS, exhibited a very small frequency asymmetry, providing weak iDMI with graphene.

These changes in the magnetic dead layer, coercive field, two-magnon scattering, and surface magnetic anisotropy can be attributed to the presence of graphene ripples. Consequently, our findings highlight the significant influence of graphene ripples on the magnetic properties of the multilayers and offer valuable insights for the design of graphene/FM structures.

Data will be made available on reasonable request.

## ACKNOWLEDGMENTS

Agence Nationale de la Recherche (ANR) and Commissariat à l'Investissement d'Avenir are gratefully acknowledged for their financial support of this paper through Labex Science and Engineering for Advanced Materials and Devices Grants No. ANR 11 LABX 086, No. ANR 11 IDEX 05 02, and No. ANR-14CE08-0018. This paper was partially supported by UParis-NUS 2020 and 2023 awards "Creating tailor-made chiral magnetic nanostructures" and "Inducing magnetic chirality without heavy metals," respectively, and Structure fédérative de recherche NAP MOSAIC of the University Sorbonne Paris Nord through MONOGRAPH-IN and INTERFER-2D projects.

The authors declare that they have no known competing financial interests or personal relationships that could have appeared to influence the work reported in this paper.

- 
- [1] M. Mansuripur, *The Physical Principles of Magneto-Optical Recording* (Cambridge University Press, Cambridge, 1995).
- [2] B. Dieny, V. S. Speriosu, S. S. P. Parkin, B. A. Gurney, D. R. Wilhoit, and D. Mauri, Giant magnetoresistive in soft ferromagnetic multilayers, *Phys. Rev. B* **43**, 1297(R) (1991).
- [3] A. Soumyanarayanan, N. Reyren, A. Fert, and C. Panagopoulos, Emergent phenomena induced by spin-orbit coupling at surfaces and interfaces, *Nature (London)* **539**, 509 (2016).
- [4] M. Belmeguenai, Y. Roussigné, S. M. Chérif, A. Stashkevich, T. Petrisor, M. Nasui, and M. S. Gabor, Influence of the capping layer material on the interfacial Dzyaloshinskii-Moriya interaction in Pt/Co/capping layer structures probed by Brillouin light scattering, *J. Phys. D: Appl. Phys.* **52**, 125002 (2019).
- [5] F. Ajejas, A. Gudín, R. Guerrero, A. A. Barcelona, J. M. Diez, L. de Melo Costa, P. Olleros, M. A. Niño, S. Pizzini, J. Vogel *et al.*, Unraveling Dzyaloshinskii-Moriya interaction and chiral nature of graphene/cobalt interface, *Nano. Lett.* **18**, 5364 (2018).
- [6] D. Odkhuu, T. Tsevelmaa, P. Taivansaikhan, N. Park, S. C. Hong, and S. H. Rhim, Tunability of magnetic anisotropy of Co on two-dimensional materials by tetrahedral bonding, *Phys. Rev. B* **99**, 014419 (2019).
- [7] H. Yang, S. O. Valenzuela, M. Chshiev, S. Couet, B. Dieny, B. Dlubak, A. Fert, K. Garello, M. Jamet, D.-E. Jeong *et al.*, Two-dimensional materials prospects for non-volatile spintronic memories, *Nature (London)* **606**, 663 (2022).
- [8] W. Han, R. K. Kawakami, M. Gmitra, and J. Fabian, Graphene spintronics, *Nat. Nanotechnol.* **9**, 794 (2014).
- [9] M. Piquemal-Banci, R. Galceran, S. M.-M. Dubois, V. Zlatko, M. Galbiati, F. Godel, M.-B. Martin, R. S. Weatherup, F. Petroff, A. Fert *et al.*, Spin filtering by proximity effects at hybridized interfaces in spin-valves with 2D graphene barriers, *Nat. Commun.* **11**, 5670 (2020).
- [10] H. Naganuma, V. Zlatko, M. Galbiati, F. Godel, A. Sander, C. Carrétéro, O. Bezencenet, N. Reyren, M.-B. Martin, B. Dlubak *et al.*, A perpendicular graphene/ferromagnet electrode for spintronics, *Appl. Phys. Lett.* **116**, 173101 (2020).
- [11] N. Rougemaille, A. T. Ndiaye, J. Coraux, C. Vo-Van, O. Fruchart, and A. K. Schmid, Perpendicular magnetic anisotropy of cobalt films intercalated under graphene, *Appl. Phys. Lett.* **101**, 142403 (2012).
- [12] A. D. Vu, J. Coraux, G. Chen, A. T. N'Diaye, A. K. Schmid, and N. Rougemaille, Unconventional magnetisation texture in graphene/cobalt hybrids, *Sci. Rep.* **6**, 24783 (2016).
- [13] A. V. Krasheninnikov, P. O. Lehtinen, A. S. Foster, P. Pyykkö, and R. M. Nieminen, Embedding transition-metal atoms in graphene: Structure, bonding, and magnetism, *Phys. Rev. Lett.* **102**, 126807 (2009).
- [14] F. Donati, L. Gagnaniello, A. Cavallin, F. D. Natterer, Q. Dubout, M. Pivetta, F. Patthey, J. Dreiser, C. Piamonteze, S. Rusponi *et al.*, Tailoring the magnetism of Co atoms on graphene through substrate hybridization, *Phys. Rev. Lett.* **113**, 177201 (2014).

- [15] F. S. Abdallah, K. Bouamama, S. Farhat, and S. M. Chérif, First-principles calculations study of the configurations, structural, electronic and magnetic properties of graphene and h-BN monolayers and bilayers adsorbed on Co(0001) surface, *Physica B Condens. Matter* **611**, 412755 (2021).
- [16] H. Yang, A. D. Vu, A. Hallal, N. Rougemaille, J. Coraux, G. Chen, A. K. Schmid, and M. Chshiev, Anatomy and giant enhancement of the perpendicular magnetic anisotropy of cobalt-graphene heterostructures, *Nano. Lett.* **16**, 145 (2016).
- [17] J. Rastikian, S. Suffit, C. Barraud, A. Bellec, V. Repain, Y. Roussigné, M. Belmeguenai, S. Farhat, L. Le Laurent, C. Barreateau *et al.*, Magnetic properties of devicelike cobalt/2D materials interfaces, *Phys. Rev. Mater.* **5**, 014004 (2021).
- [18] M. Belmeguenai, M. S. Gabor, F. Zighem, N. Challab, T. Petrisor, R. B. Mos, and C. Tiusan, Ferromagnetic-resonance-induced spin pumping in  $\text{Co}_{20}\text{Fe}_{60}\text{B}_{20}/\text{Pt}$  systems: Damping investigation, *J. Phys. D: Appl. Phys.* **51**, 045002 (2018).
- [19] S. Sinha, S. Pan, S. Choudhury, J. Sinha, and A. Barman, Extrinsic spin-orbit coupling-induced large modulation of Gilbert damping coefficient in CoFeB thin film on the graphene stack with different defect density, *J. Phys. Chem. C* **121**, 17442 (2017).
- [20] A. K. Mondal, S. Majumder, S. Sahoo, S. N. Panda, S. Sinha, and A. Barman, Defect-density- and Rashba-shift-induced interfacial Dzyaloshinskii-Moriya interaction and spin pumping in single-layer graphene/ $\text{Co}_{20}\text{Fe}_{60}\text{B}_{20}$  heterostructures: Implications for new-generation spintronics, *ACS Appl. Nano. Mater.* **5**, 5056 (2022).
- [21] H. Yang, G. Chen, A. A. C. Cotta, A. T. N'Diaye, S. A. Nikolaev, E. A. Soares, W. A. A. Macedo, K. Liu, A. K. Schmid, A. Fert *et al.*, Significant Dzyaloshinskii-Moriya interaction at graphene-ferromagnet interfaces due to the Rashba effect, *Nat. Mater.* **17**, 605 (2018).
- [22] B. El-Kerdi, A. Thiaville, S. Rohart, S. Panigrahy, N. Brás, J. Sampaio, and A. Mougin, Evidence of strong Dzyaloshinskii-Moriya interaction at the cobalt/hexagonal boron nitride interface, *Nano. Lett.* **23**, 3202 (2023).
- [23] W. Bao, F. Miao, Z. Chen, H. Zhang, W. Jang, C. Dames, and C. N. Lau, Controlled ripple texturing of suspended graphene and ultrathin graphite membranes, *Nat. Nanotechnol.* **4**, 562 (2009).
- [24] S. Deng and V. Berry, Wrinkled, rippled and crumpled graphene: An overview of formation mechanism, electronic properties, and applications, *Mater. Today* **19**, 197 (2016).
- [25] R. Peierls, Quelques propriétés typiques des corps solides, *Annales De L'I.H.P.* **5**, 177 (1935).
- [26] D. R. Nelson and L. Peliti, Fluctuations in membranes with crystalline and hexatic order, *J. Phys. France* **48**, 1085 (1987).
- [27] A. Fasolino, J. H. Los, and M. I. Katsnelson, Intrinsic ripples in graphene, *Nat. Mater.* **6**, 858 (2007).
- [28] J. C. Meyer, A. K. Geim, M. I. Katsnelson, K. S. Novoselov, T. J. Booth, and S. Roth, The structure of suspended graphene sheets, *Nature (London)* **446**, 60 (2007).
- [29] M. Ishigami, J. H. Chen, W. G. Cullen, M. S. Fuhrer, and E. D. Williams, Atomic structure of graphene on  $\text{SiO}_2$ , *Nano. Lett.* **7**, 1643 (2007).
- [30] K. K. Bai, Y. Zhou, H. Zheng, L. Meng, H. Peng, Z. Liu, J. C. Nie, and L. He, Creating one-dimensional nanoscale periodic ripples in a continuous mosaic graphene monolayer, *Phys. Rev. Lett.* **113**, 086102 (2014).
- [31] K. Pashova, E. Dhaouadi, I. Hinkov, O. Brinza, Y. Roussigné, M. Abderrabba, and S. Farhat, Graphene synthesis by inductively heated copper foils: Reactor design and operation, *Coatings* **10**, 305 (2020).
- [32] E. Dhaouadi, I. Hinkov, K. Pashova, N. Challab, Y. Roussigné, M. Abderrabba, and S. Farhat, Computer-aided design of graphene and 2D materials synthesis via magnetic inductive heating of 11 transition metals, *J. Phys. D: Appl. Phys.* **55**, 105302 (2022).
- [33] E. Dhaouadi, W. Alimi, M. Konstantakopoulou, I. Hinkov, M. Abderrabba, and S. Farhat, Graphene synthesis by electromagnetic induction heating of oxygen-rich copper foils, *Diam. Relat. Mater.* **132**, 109659 (2023).
- [34] F. R. Bagsican, A. Winchester, S. Ghosh, X. Zhang, L. Ma, M. Wang, H. Murakami, S. Talapatra, R. Vajtai, P. M. Ajayan *et al.*, Adsorption energy of oxygen molecules on graphene and two-dimensional tungsten disulfide, *Sci. Rep.* **7**, 1774 (2017).
- [35] S. M. Chérif, Y. Roussigné, and P. Moch, Effect of anisotropy on Brillouin spectra of stripe-structured cobalt layers, *Phys. Rev. B* **59**, 9482 (1999).
- [36] K. Di, V. L. Zhang, H. S. Lim, S. C. Ng, M. H. Kuok, J. Yu, J. Yoon, X. Qiu, and H. Yang, Direct observation of the Dzyaloshinskii-Moriya interaction in a Pt/Co/Ni film, *Phys. Rev. Lett.* **114**, 047201 (2015).
- [37] M. Belmeguenai, J. P. Adam, Y. Roussigné, S. Eimer, T. Devolder, J.-V. Kim, S. M. Cherif, A. Stashkevich, and A. Thiaville, Interfacial Dzyaloshinskii-Moriya interaction in perpendicularly magnetized Pt/Co/ $\text{AlO}_x$  ultrathin films measured by Brillouin light spectroscopy, *Phys. Rev. B* **91**, 180405(R) (2015).
- [38] M. Belmeguenai, H. Tuzcuoglu, M. S. Gabor, T. Petrisor, C. Tiusan, D. Berling, F. Zighem, T. Chauveau, S. M. Chérif, and P. Moch,  $\text{Co}_2\text{FeAl}$  thin films grown on MgO substrates: Correlation between static, dynamic, and structural properties, *Phys. Rev. B* **87**, 184431 (2013).
- [39] M. S. Poorali and M. M. Bagheri-Mohagheghi, Synthesis and physical properties of multi-layered graphene sheets by arc-discharge method with  $\text{TiO}_2$  and ZnO catalytic, *J. Mater. Sci. Mater. in Electronics* **28**, 6186 (2017).
- [40] K. S. Subrahmanyam, S. R. C. Vivekchand, A. Govindaraj, and C. N. R. Rao, A study of graphenes prepared by different methods: Characterization, properties and solubilization, *J. Mater. Chem.* **18**, 1517 (2008).
- [41] E. K. Athanassiou, R. N. Grass, and W. J. Stark, Large-scale production of carbon-coated copper nanoparticles for sensor applications, *Nanotechnol.* **17**, 1668 (2006).
- [42] Y. Y. Wang, Z. H. Ni, Z. X. Shen, H. M. Wang, and Y. H. Wu, Interference enhancement of Raman signal of graphene, *Appl. Phys. Lett.* **92**, 043121 (2008).
- [43] N. Ferralis, Probing mechanical properties of graphene with Raman spectroscopy, *J. Mater. Sci.* **45**, 5135 (2010).
- [44] A. Reina, X. Jia, J. Ho, D. Nezich, H. Son, V. Bulovic, M. S. Dresselhaus, and K. Jing, and Large Area, Few-layer graphene films on arbitrary substrates by chemical vapor deposition, *Nano. Lett.* **9**, 30 (2009).
- [45] Z. H. Ni, H. M. Wang, Y. Ma, J. Kasim, Y. H. Wu, and Z. X. Shen, Tunable stress and controlled thickness modification in graphene by annealing, *ACS Nano* **2**, 1033 (2008).



- [46] A. W. Robertson and J. H. Warner, Hexagonal single crystal domains of few-layer graphene on copper foils, *Nano. Lett.* **11**, 1182 (2011).
- [47] *Magnetism: Fundamentals*, edited by E. du Trémolet de Lacheisserie, D. Gignoux, and M. Schlenker (Springer, New York, 2003).
- [48] A. J. Berger, W. Amamou, S. P. White, R. Adur, Y. Pu, R. K. Kawakami, and P. C. Hammel, Magnetization dynamics of cobalt grown on graphene, *J. Appl. Phys.* **115**, 17C510 (2014).
- [49] C. Du, H. Wang, F. Yang, and P. C. Hammel, Systematic variation of spin-orbit coupling with  $d$ -orbital filling: Large inverse spin Hall effect in  $3d$  transition metals, *Phys. Rev. B* **90**, 140407(R) (2014).
- [50] Q. Jiang, H. N. Yang, and G. C. Wang, Effect of interface roughness on hysteresis loops of ultrathin Co films from 2 to 30 ML on Cu(001) Surfaces, *Surf. Sci.* **373**, 181 (1997).
- [51] S. Y. Jang, C. Y. You, S. H. Lim, and S. R. Lee, Annealing effects on the magnetic dead layer and saturation magnetization in unit structures relevant to a synthetic ferrimagnetic free structure, *J. Appl. Phys.* **109**, 013901 (2011).
- [52] Y. H. Wang, W. C. Chen, S. Y. Yang, K. H. Shen, C. Park, M. J. Kao, and M. J. Tsai, Interfacial and annealing effects on magnetic properties of CoFeB thin films, *J. Appl. Phys.* **99**, 08M307 (2006).
- [53] C. F. Pai, M. H. Nguyen, C. Belvin, L. H. Vilela-Leão, D. C. Ralph, and R. A. Buhrman, Enhancement of perpendicular magnetic anisotropy and transmission of spin-Hall-effect-induced spin currents by a Hf spacer layer in W/Hf/CoFeB/MgO layer structures, *Appl. Phys. Lett.* **104**, 082407 (2014).
- [54] D. Jhahria, D. K. Pandya, and S. Chaudhary, Orbital moment probed spin orbit coupling effects on anisotropy and damping in CoFeB thin films, *RSC. Adv.* **6**, 94717 (2016).
- [55] J. S. Kim, G. Kim, J. Jung, K. Jung, J. Cho, W. Y. Kim, and C. Y. You, Control of crystallization and magnetic properties of CoFeB by boron concentration, *Sci. Rep.* **12**, 4549 (2022).
- [56] B. Dieny and A. Vedyayev, Crossover from easy-plane to perpendicular anisotropy in magnetic thin films: Canted anisotropy due to partial coverage or interfacial roughness, *Europhys. Lett.* **25**, 723 (1994).
- [57] H. Bouloussa, R. Ramaswamy, Y. Roussigné, A. Stashkevich, H. Yang, M. Belmeguenai, and S. M. Chérif, Pt concentration dependence of the interfacial Dzyaloshinskii-Moriya interaction, the Gilbert damping parameter and the magnetic anisotropy in Py/Cu<sub>1-x</sub>Pt<sub>x</sub> systems, *J. Phys. D: Appl Phys* **52**, 055001 (2019).
- [58] M. Belmeguenai, D. Apalkov, Y. Roussigné, M. Chérif, A. Stashkevich, G. Feng, and X. Tang, Exchange stiffness and damping constants in diluted Co<sub>x</sub>Fe<sub>y</sub>B<sub>1-x-y</sub> thin films, *J. Phys. D: Appl. Phys.* **50**, 415003 (2017).
- [59] I. Benguetat-El Mokhtari, D. Ourdani, Y. Roussigné, R. B. Mos, M. Nasui, S. M. Chérif, A. Stachkevich, M. S. Gabor, and M. Belmeguenai, Investigation of the correlation between perpendicular magnetic anisotropy, spin mixing conductance and interfacial Dzyaloshinskii-Moriya interaction in CoFeB-based systems, *J. Phys. D: Appl. Phys.* **53**, 505003 (2020).
- [60] S. M. Dunaevskii, E. Y. Lobanova, E. K. Mikhaïlenko, and I. I. Pronin, Magnetic anisotropy of graphene-coated thin iron films, *Phys. Solid State* **61**, 1310 (2019).
- [61] P. Bruno, Dipolar magnetic surface anisotropy in ferromagnetic thin films with interfacial roughness, *J. Appl. Phys.* **64**, 3153 (1988).
- [62] See Supplemental Material at <http://link.aps.org/supplemental/10.1103/PhysRevMaterials.8.014410> for the MS-FMR measurements of effective magnetization, the comparison with BLS measurements, and the measurements of magnetic damping using MS-FMR.
- [63] J. H. Moon, S. M. Seo, K. J. Lee, K. W. Kim, J. Ryu, H. W. Lee, R. D. McMichael, and M. D. Stiles, Spin-wave propagation in the presence of interfacial Dzyaloshinskii-Moriya interaction, *Phys. Rev. B* **88**, 184404 (2013).
- [64] A. K. Chaurasiya, A. Kumar, R. Gupta, S. Chaudhary, P. K. Muduli, and A. Barman, Direct observation of unusual interfacial Dzyaloshinskii-Moriya interaction in graphene/NiFe/Ta heterostructures, *Phys. Rev. B* **99**, 035402 (2019).
- [65] A. Belabbes, G. Bihlmayer, F. Bechstedt, S. Blügel, and A. Manchon, Hund's rule-driven Dzyaloshinskii-Moriya interaction at  $3d - 5d$  interfaces, *Phys. Rev. Lett.* **117**, 247202 (2016).
- [66] C. Moreau-Luchaire, C. Moutafis, N. Reyren, J. Sampaio, C. A. F. Vaz, N. Van Horne, K. Bouzehouane, K. Garcia, C. Deranlot, P. Warnicke *et al.*, Additive interfacial chiral interaction in multilayers for stabilization of small individual skyrmions at room temperature, *Nat. Nanotechnol.* **11**, 444 (2016).
- [67] A. S. Samardak, A. V. Davydenko, A. G. Kolesnikov, A. Y. Samardak, A. G. Kozlov, B. Pal, A. V. Ognev, A. V. Sadovnikov, S. A. Nikitov, A. V. Gerasimenko *et al.*, Enhancement of perpendicular magnetic anisotropy and Dzyaloshinskii-Moriya interaction in thin ferromagnetic films by atomic-scale modulation of interfaces, *NPG Asia Mater.* **12**, 51 (2020).
- [68] L. Zhu, D. C. Ralph, and R. A. Buhrman, Effective spin-mixing conductance of heavy-metal-ferromagnet interfaces, *Phys. Rev. Lett.* **123**, 057203 (2019).
- [69] X. Liu, W. Zhang, M. J. Carter, and G. Xiao, Ferromagnetic resonance and damping properties of CoFeB thin films as free layers in MgO-based magnetic tunnel junctions, *J. Appl. Phys.* **110**, 033910 (2011).
- [70] I. Benguetat-El Mokhtari, Y. Roussigné, S. M. Chérif, A. Stashkevich, S. Auffret, C. Baraduc, M. Gabor, H. Béa, and M. Belmeguenai, Interface phenomena in ferromagnet/TaO<sub>x</sub>-based systems: Damping, perpendicular magnetic anisotropy, and Dzyaloshinskii-Moriya interaction, *Phys. Rev. Mater.* **4**, 124 (2020).